OPEN

Correspondence and
requests for materials
should be addressed to
T.W. (t.wang@
sheffield.ac.uk)

Room temperature continuous–wave green lasing from an InGaN microdisk on silicon

M. Athanasiou, R. Smith, B. Liu & T. Wang

Department of Electronic and Electrical Engineering, University of Sheffield, Mappin Street, Sheffield, S1 3JD, United Kingdom.

Optically pumped green lasing with an ultra low threshold has been achieved using an InGaN/GaN based micro-disk with an undercut structure on silicon substrates. The micro-disks with a diameter of around 1 µm were fabricated by means of a combination of a cost-effective silica micro-sphere approach, dry-etching and subsequent chemical etching. The combination of these techniques both minimises the roughness of the sidewalls of the micro-disks and also produces excellent circular geometry. Utilizing this fabrication process, lasing has been achieved at room temperature under optical pumping from a continuous-wave laser diode. The threshold for lasing is as low as 1 kW/cm². Time–resolved micro photoluminescence (PL) and confocal PL measurements have been performed in order to further confirm the lasing action in whispering gallery modes and also investigate the excitonic recombination dynamics of the lasing.

The last four decades have seen unparalleled impact of the semiconductor industry driven by silicon technology. Silicon based technologies are extremely mature and cost-effective, however, it is well-known that silicon exhibits an indirect band structure prohibiting the use of silicon as a light emitter. The unification of III–V technologies with silicon technology would therefore be an ideal solution to allow the integration of semiconductor based electronics and photonics. Therefore, the fabrication of silicon compatible III-nitride optoelectronics, namely, III-nitride optoelectronics on silicon substrates, would perfectly meet the requirements. This is particularly important for III-nitride based optoelectronics due to the significantly more complicated device fabrication techniques required for III-nitrides compared to other III–V semiconductors. This would not only eliminate their individual fundamental limits but also draw together the major advantages from the two families of semiconductors. However, a number of great challenges exist in epitaxial growth due to the large lattice-mismatch and large difference in thermal expansion coefficients of silicon and GaN, leading to less competitive performance compared with their counterparts on widely used sapphire substrates. To date, there are no reports of lasing from III-nitrides on silicon in the green spectral region.

Micro- or nano-cavities, such as photonic crystal cavities[1,2], plasmonic waveguides[3–7], have been demonstrated for the fabrication of laser structures with excellent performance. Micro-disk lasers have become increasingly attractive over the last decade due to their simple geometry and their compact size[8–10]. Micro-disk lasers can be used to provide high quality whispering gallery modes (WGMs), leading to low threshold lasing. This is particularly important for III-nitride based lasers, as III-nitride laser diodes (LDs) exhibit intrinsically much higher thresholds for lasing than other III–V semiconductor LDs. This is to a large degree an intrinsic limitation due to the high carrier densities of states resulting from the high effective masses in wide bandgap materials. Furthermore, micro-disk lasers on Si substrates can be potentially used to integrate electronics and photonics on the same wafer, meeting the challenges of fabricating photonic-electronic integrated circuits for communication and computation technologies in order to overcome their fundamental limits in speed and bandwidth[11]. In this case, taking the extremely mature silicon technology into account, III-nitrides on silicon exhibit overwhelming advantages compared with widely used GaN-on-sapphire technology for the fabrication of micro-disk lasers. For instance, the utilisation of silicon as substrates allows the formation of an undercut structure, which is necessary for micro-disks, but does not require growth of extra sacrificial layers, which are necessary to fabricate GaN-based micro-disks on sapphire substrates[9,10], as it is extremely difficult to chemically etch sapphire. Additionally, the growth of these extra sacrificial layers could potentially cause degradation in crystal quality based on GaN-on-sapphire.

Current GaN-based micro-disks suffer from some serious fabrication problems, such as inclined sidewalls and non-uniformity in circularity[12,13], leading to major limits in their optical performance. The situation for fabrication of GaN micro-disks on sapphire is even worse, as the extra sacrificial layers mentioned above are required in order to form an undercut structure or even more complicated distributed Bragg reflectors are required[9,10,14]. Both aim to enhance the optical confinement along the vertical direction in order to minimise light leakage.

In this work, we report the first green lasing on silicon substrate in continuous wave (cw) mode at room temperature. The lasing is from a single microdisk, consisting of 5 pairs of InGaN/GaN multiple quantum wells (MQW) as an emitting region grown on silicon, optically pumped using a cw diode laser. The threshold for lasing is as low as ~ 1 kW/cm². The single micro-disk laser was fabricated by means of combining a cost-effective approach using microspheres and a simple dry-etching technique, where the undercut structure below the micro-disk region was formed by chemical etching made possible by taking advantage of the growth of the structure on silicon.

The InGaN/GaN MQW micro-disks used in the present study were fabricated from a standard epi-wafer of 5 periods InGaN/GaN MQWs grown on (111) silicon by using a standard metal organic chemical vapour deposition (MOCVD) technique. The details of the InGaN/GaN MQW wafer are schematically described in Figure 1a, where the indium content in each quantum well is around 27%, and the thicknesses of InGaN quantum well and GaN barrier are 2.5 nm and 10 nm, respectively. The micro-disk cavity is fabricated using a cost effective micro-sphere lithography approach (see supplementary information for the details of the fabrication) which is basically identical to the established silica nanosphere lithography technique[15,16]. The micro-disk is schematically defined in Figure 1b. The formation of the undercut structure can be achieved by simple chemical etching, leading to an air gap under the micro-

disk region, as silicon can be easily chemically etched using potassium hydroxide (KOH)[14]. The introduction of the air gap is expected to enhance the optical confinement in the micro-disk region along the vertical direction.

Figure 1c displays a typical side-view scanning electron microscopy (SEM) image of our fabricated micro-disk, exhibiting the straight and smooth sidewalls and the large air gap underneath. The air-gap below the micro-disk is approximately ~ 1.2 μm height, which is much larger than that obtained in the micro-disks fabricated based on GaN-on sapphire, where the extra sacrificial layer with a total thickness of ~ 200 nm is used[9,10]. The very large air-gap is expected to minimise any optical losses to the silicon substrate and thus is expected to significantly enhance the optical confinement along the vertical direction[17]. A top view SEM image is provided in the inset of Figure 1c, showing the circular geometry of the micro-disk with a diameter of around 1 μm. Figure 1d shows a SEM image with a higher magnification, indicating perfectly smooth sidewalls. A smooth sidewall is crucial to achieving excellent performance of micro-disk lasers[9]. Any roughness of the sidewalls of a micro-disk is expected to result in the leakage of optical modes and thus cause an increase in threshold for lasing, as it will cause a disruption of light propagation in WGM. In order to minimise any potential damage or defects (potential non-radiative recombination centres) generated during the dry etching process, a surface treatment was carried out. The process we have developed involves the utilisation of hot nitric acid (detailed in the supplementary material), and has been employed in the fabrication of our III-nitride based plasmonic nano-lasers, demonstrating massive improvement in optical properties[7].

The utilisation of all of the above processes offers a significantly enhanced chance of achieving cw green lasing at room temperature. Figure 2a shows the typical lasing spectra of our micro-disk laser measured at room temperature as a function of optical pumping power density from 79 W/cm² to 25 kW/cm², excited using a 405 nm cw diode laser in a micro-PL system. This system is equipped
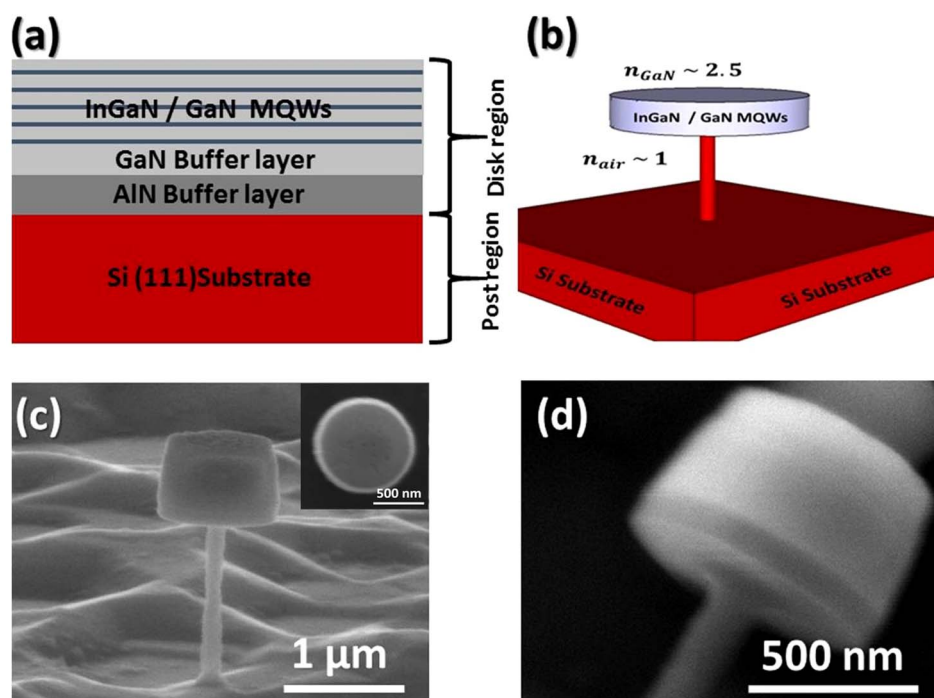

Figure 1 | (a) Schematic illustration of InGaN/GaN MQW epi-wafer grown on a (111) silicon substrate, which is used to fabricate our micro-disk lasers. The thicknesses of the AlN and GaN buffer layers are 200 and 500 nm respectively; the quantum wells are 2.5 nm and barriers 10 nm; (b) Schematic diagram of our micro-disk laser, where this structure leads to light propagating in whispering gallery modes around the periphery of the micro-disk; (c) Typical side-view SEM image with a top view SEM image given in an inset showing the micro-disk with a diameter of ~ 1 μm; (d) Side-view SEM image of the micro-disk after wet chemical etching under a higher magnification.
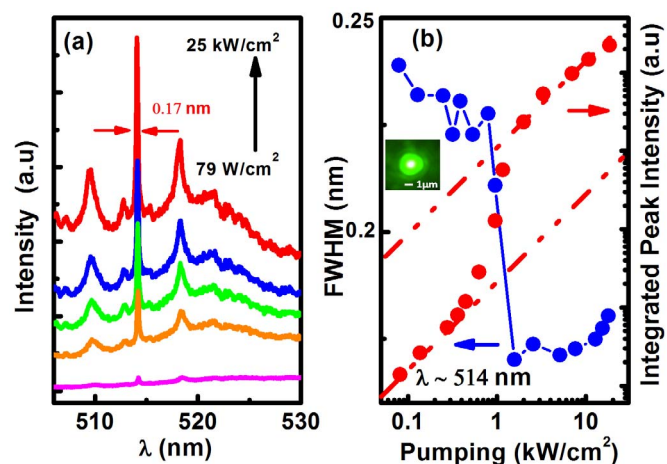
Figure 2 | (a) Lasing spectra from our micro-disk laser recorded as a function of optical pumping power density at room temperature; (b) L–L curve plotted in a log-log scale and FWHM as a function of optical pumping power density, respectively. The dashed-lines are guides for the eye. The inset shows the lasing image of the micro-disk, captured above the threshold.

with a high resolution camera and a nanometre resolution positioner, allowing us to identify and address single micro-disks accurately. Under low excitation power, a few weak emission peaks (different WGMs) have been observed. However, when the optical pumping power density is above 1 kW/cm², a very sharp and strong emission peak at 514 nm has been observed. The intensity increases dramatically along with a significant reduction in full width at half maximum (FWHM) with further increase in optical pumping power density. The thickness of the microdisk is larger than $\lambda/2n$, giving the potential of some weak vertical or hybrid modes, and thus one can observe other peaks in Figure 2a.

Figure 2b shows a light-light (L–L) plot of the lasing mode at 514 nm, described in a log-log scale. The L–L curve exhibits an "s" shaped behaviour, a typical fingerprint for lasing[3–7,18,19]. The threshold for lasing can be determined from the L–L plot, which is 1 kW/cm². Figure 2b shows the FWHM of the emission peak as function of optical pumping power density, exhibiting a dramatic reduction with increasing optical pumping power density which starts from 1 kW/cm². The FWHM drops down to 0.17 nm from 0.24 nm with increasing optical pumping power density, further confirming the lasing behaviour. The quality factor (Q factor), defined as $\lambda/\Delta\lambda$, can be evaluated, where λ and $\Delta\lambda$ are the central emission wavelength and FWHM, respectively. Below threshold, the Q factor is ~2150. The high Q factor achieved could be partially attributed to the enhancement in optical confinement along the vertical direction[10,17] as a result of the much larger air-gap obtained below the micro-disk due to the major benefit of using a silicon substrate. This also leads to the enhancement in the coupling between the cavity mode and the green emission from the InGaN/GaN MQWs. Further characterisation of the micro-disk laser allows the β factor, defined as the fraction of spontaneous emission coupled into the lasing mode, to be determined based on the evaluation of the ratio of the integrated intensity below and above lasing threshold from the L–L curve[20]. The β factor of 0.043 can be obtained based on a fitting using a standard rate equation analysis[21,22]. Inset of Figure 2b shows an optical image of the lasing from the micro-disk, captured by a CCD camera when the optical pumping is above the threshold.

Further examination of Figure 2b shows a slight increase in FWHM of the lasing peaks when the optical pumping power density exceeds 10 kW/cm². This phenomenon along with a slight red-shift in the lasing peak is due to thermal effects under high excitation powers[19].
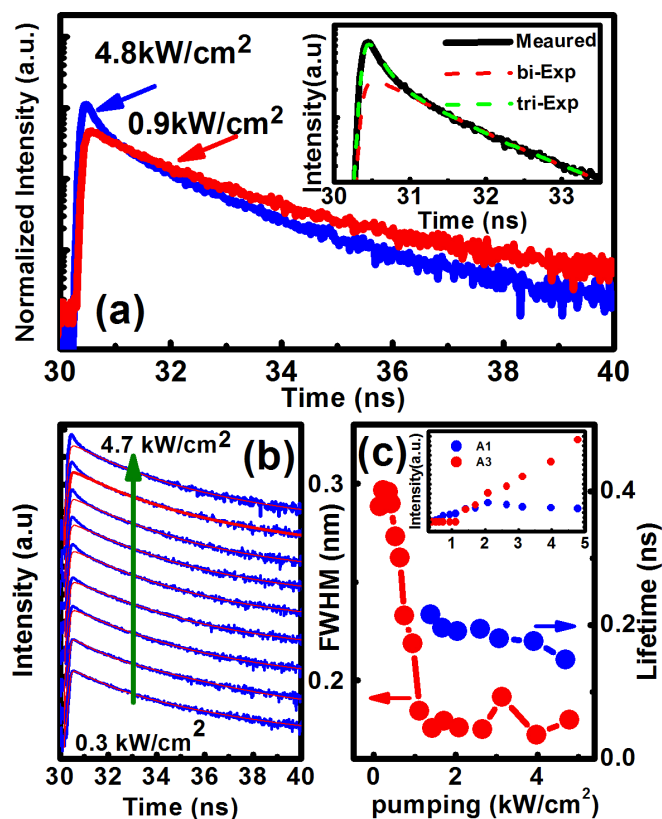

Figure 3 | (a) µ-TRPL decay traces of our micro-disk laser recoded at room temperature above and below the threshold, respectively. The inset shows the data-fitting using the bi-exponential and tri-exponential model in order to compare with µ-TRPL decay trace measured above the threshold; (b) Dependence of µ-TRPL decay traces of our micro-disk laser on optical pumping power density, showing the evolution from spontaneous emission to lasing; (c) FWHM of the lasing peak and lifetime of the ultra-fast decay component as a function of optical pumping power density. The inset shows A_1 and A_3 coefficients as a function of optical pumping power density.

In order to further investigate the lasing oscillation of our micro-disk, time resolved micro-PL (µ-TRPL) measurements have been performed on the single micro-disk at room temperature as a function of optical pumping power density, where a 375 nm pulsed diode laser with a pulse width of 50 ps was used as an optical pumping source. Figure 3a shows the µ-TRPL decay traces measured below the threshold (0.9 kW/cm²) and above the threshold (4.7 kW/cm²) as examples, demonstrating a major difference between them. Above the threshold, an extra ultra-fast decay component has been observed, and can be seen more clearly after data-fitting.

A standard bi-exponential model was used to fit the TRPL decay trace below the threshold[23–25], the TRPL traces [I(t)] can be described by Equation (1) below,

$$I(t) = A_1 \exp(-t/\tau_1) + A_2 \exp(-t/\tau_2) \qquad (1)$$

where A_1 and τ_1 (A_2 and τ_2) represent the fast (slow) decay components. The fitting results are plotted in dashed lines shown in Figure 3a in a similar way as we did previously on different structures[24,25]. The lifetimes of the fast and slow decay components obtained are around 1.0 ns and 2.7 ns, respectively.

In a remarkable contrast, the bi-exponential model no longer works for the TRPL traces obtained above the threshold (4.7 kW/cm² as an example for Figure 3a). In that case, an extra decay component is required in order to fit the TRPL trace. Therefore, an extra term is required in Equation 1 as shown below:

$$I(t) = A_1 \exp\left(-t/\tau_1\right) + A_2 \exp\left(-t/\tau_2\right) + A_3 \exp\left(-t/\tau_3\right) \quad (2)$$

where A_1 and τ_1 (A_2 and τ_2) remain unchanged as stated above, and the last term represents the extra component, which is due to laser action[26,27]. For comparison, the fitting based on both the bi-exponential model and the tri-exponential model has been performed, and is shown in the inset of Figure 3a. A good fit using the tri-exponential model (shown as green colour) has been obtained, while the bi-exponential model (shown as red colour) no longer works. The extra component (i.e., τ_3) is extremely fast, at ~150 ps, which approaches the system response-time, while the lifetimes of τ_1 and τ_2 remain approximately unchanged and are ~1.10 ns and ~2.72 ns respectively. The ultra-fast decay component is due to lasing action[26,27], providing solid evidence for lasing observed from our micro-disk laser.

Figure 3b shows the μ-TRPL traces of the micro-disk laser recorded as a function of optical pumping power density from 0.3 to 4.7 kW/cm² in order to observe the evolution from spontaneous emission to lasing and also determine a threshold for lasing. Figure 3b clearly indicates that the ultra-fast component appears only when the optical pumping power density is above ~1 kW/cm², the threshold which has been obtained based on Figure 2. In Figure 3b, the bi-exponential model was deliberately used to fit the TRPL traces (red lines) in order to observe the evolution of the appearance of the ultra-fast component clearly. When the optical pump power density is below 1 kW/cm², the TRPL decay can be fit well by the bi-exponential model, while the ultra-fast component starts to appear and then becomes dominant when the optical pump power density is above 1 kW/cm². It becomes even more clear if we plot the FWHM of the lasing peak at 514 nm and the lifetime of the ultra-fast decay component (i.e., τ_3) as a function of optical pumping power density in a same figure, which is Figure 3c. It is clear that the sudden reduction in FWHM and the appearance of the ultra-fast component take place simultaneously, i.e., above the threshold. It should be noted that the optical pumping power density dependent FWHM shown in Figure 3c is obtained using a 375 nm pulsed laser as an optical pumping source, thus leading to less significant thermal effects compared with those using a 405 nm cw diode laser as an optical pumping source for Figure 2b. As a result, Figure 3c is slightly different from the data shown in Figure 2b.

The inset of Figure 3c provides the comparison of the ultra-fast decay component (i.e., lasing part described as A_3 shown in Equation 2) and the standard fast decay component (i.e., spontaneous part, described as A_1 shown in Equation 2). When the optical pumping power density exceeds the threshold (i.e., 1 kW/cm²), A_3 increases very quickly and then eventually overtakes A_1. This means that the lasing dominates the emission when the optical pumping power density is above the threshold. Please note that for simplicity we label A_3 as zero below the threshold, as the ultrafast component does not appear below the threshold.

Spatially resolved PL measurements were performed at room temperature using a commercial confocal PL system for further investigation of our micro-disk laser. The spatial resolution of the system is approximately ~160 nm, where a 375 nm cw diode laser was used as an excitation source. Figure 4a shows the lasing spectrum above the threshold, where the highlighted areas labelled with blue and red colour represent the on- (i.e., lasing peak at 514 nm) and off-resonance regions, respectively. Figure 4b shows a typical confocal PL mapping image of the micro-disk for the off-resonance case (i.e., red-colour), where the boundary of the micro-disk is defined by white dashed circles. In the case of the off-resonance emission, the light is mainly due to spontaneous emission with random phase. Figure 4c shows a typical confocal PL image for the on-resonance case, demonstrating that the coherent light circulating around the periphery of the micro-disk to form clear WGMs[28–32]. Standard finite difference time domain (FDTD) simulations have been performed to confirm
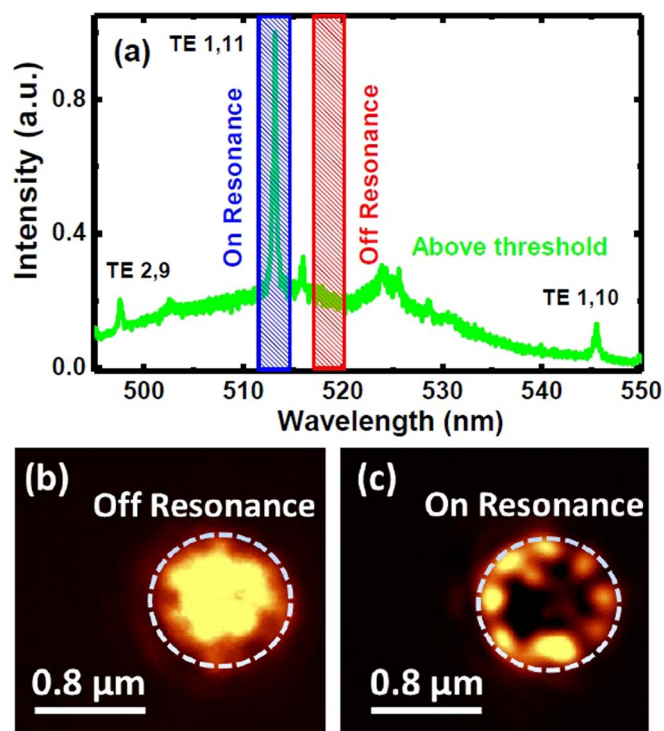

Figure 4 | (a) Lasing spectrum of our micro-disk laser above the threshold with blue and red colors highlighting the regions for the on- and off-resonance; (b) Typical confocal PL image for the off-resonance case; (c) Typical confocal PL image for the on-resonance case.

the WG mode at 514 nm, agreeing well with the observed micro-disk spectrum as shown in Figure 2a. The modes are labelled in Figure 4a.

In summary, we have reported room temperature green lasing on silicon with an ultra low threshold from InGaN/GaN MQW micro-disk laser with a undercut structure, which was fabricated by means of a cost-effective micro-sphere approach with subsequent dry-etching and chemical etching. The optically pumped lasing at 514 nm has been achieved with a cw diode laser as an optical pumping source. The threshold for lasing is as low as approximately 1 kW/cm². This is the first report of a green laser on silicon substrate so far. Optical pumping power dependent measurements have confirmed the lasing action. Further evidence includes time resolved micro-PL measurements, demonstrating an ultrafast decay component with a lifetime of ~150 ps due to the lasing action when the optical pumping power density is above the threshold. This result is in a good agreement with the optical pumping power dependent measurements. Confocal PL mapping measurements have been performed, demonstrating a clear coupling of coherent light with the WG mode.

Methods

Fabrication of microdisk laser. The micro-disks were fabricated from a standard InGaN/GaN MQW epi-wafer, which was grown by MOCVD on a (111) silicon substrate. We modified and applied our high temperature AlN buffer approach which was originally developed for the growth of GaN on sapphire to the growth of GaN on Si[32–35]. The epi-wafer consists of 200 nm AlN buffer followed by a 500 nm GaN buffer both grown at high temperatures, then 5 pairs of $In_{0.27}Ga_{0.83}N$/GaN MQWs with the barrier and the well thickness of 2.5 and 10 nm respectively, and finally a 10 nm GaN capping layer. The epi-wafer was then fabricated into single micro-disk structures by a combination of a silica microsphere approach, and dry etching and subsequent chemical etching. Initially, the silica particles with a diameter of approximately 1 μm were diluted in DI water with 1 : 50 concentration and then deposited directly on the surface of the InGaN/GaN MQW epi-wafer using a spin-coating method at a high rotation speed (7000 rpm), to serve as micro-masks for subsequent dry etching. A standard inductively coupled plasma (ICP) technique was used to etch the InGaN/GaN epi-wafer to form sparsely distributed micro pillars. Silica microspheres were then removed from the top of the pillars simply by using an ultrasonic bath. Finally, a KOH wet etching method was then employed to undercut the micro-disk and

introduce an air gap, which isolates the micro-disk region from the silicon substrate. A large air-gap (~1.2 μm) with a very small post remaining to mechanically support the micro-disk was formed under the micro-disk region, significantly enhancing the light confinement along the vertical direction and thus minimising any optical losses to silicon substrate. A further surface treatment involving the utilisation of hot nitric acid has been employed in order to remove the residual etchants and the damage generated during the ICP dry etching process. The detailed process for the fabrication of our InGaN/GaN micro-disks is schematically shown in Supplementary Fig. S1.

Lasing spectra. Lasing spectral measurements were performed using a micro-PL system. A 405 nm continuous wave (cw) diode laser was used as an optical pumping source and a monochromator (Horiba IHR550) equipped with an air-cooled charge coupled device (CCD). An objective lens (50×, NA = 0.43) was used to focus the laser beam down to a spot with a diameter <2 μm. The emission spectra were recorded by the monochromator with a resolution of 0.01 nm. All of the measurements were performed at room temperature.

Time resolved micro photoluminescence. Time resolved micro photoluminescence measurements were carried out by the above micro-PL system equipped with a time-correlated single photon counting (TCSPC) system. A 375 nm pulsed diode laser with a pulse width of 50 picoseconds (ps) was used as an excitation source, and luminescence was dispersed by the monochromator and detected by a Hamamatsu hybrid photon counting PMT. The system response-time is 150 ps. The average excitation power with a pulse repetition of 10 MHz is 0.15 mW, and the same objective lens (50×, NA = 0.43) described above was used to focus the laser beam down to a spot with a diameter < 2 μm.

1. Shambat, G. *et al.* Ultrafast direct modulation of a single-mode photonic crystal nanocavity light-emitting diode. *Nat. Commun.* **2**, 539 (2011).
2. Jeong, K. Y. *et al.* Electrically driven nanobeam laser. *Nat. Commun.* **4**, 2822 (2013).
3. Noginov, M. A. *et al.* Demonstration of a spaser-based nanolaser. *Nature* **460**, 1110–1112 (2009).
4. Oulton, R. F. *et al.* Plasmon lasers at deep subwavelength scale. *Nature* **461**, 629–632 (2009).
5. Ma, R. M. *et al.* Room-temperature sub-diffraction-limited plasmon laser by total internal reflection. *Nat. Mater.* **10**, 110–113 (2011).
6. Lu, Y. L. *et al.* Plasmonic nanolaser using epitaxially grown silver film. *Science* **337**, 450 (2012).
7. Hou, Y. *et al.* Room temperature plasmonic lasing from a single nanorod with low threshold. *Sci. Rep.* **4**, 5014 (2014).
8. Kim, Y. H. *et al.* Graphene-contact electrically driven microdisk lasers. *Nat. Commun.* **3**, 1123 (2012).
9. Adele, C. *et al.* Room-temperature continuous-wave lasing in GaN/InGaN microdisks. *Nat. Photon.* **1**, 61–64 (2007).
10. Aharonovich, I. *et al.* Low threshold, room-temperature microdisk lasers in the blue spectral range. *Appl. Phys. Lett.* 103, 021112 (2013).
11. Vahal, K. J. Optical microcavities. *Nature* **424**, 839–846 (2003).
12. Choi, H. W. *et al.* Lasing in GaN microdisks pivoted on Si. *Appl. Phys. Lett.* **89**, 211101 (2006).
13. Lee, K. J. *et al.* Optical properties of InGaN/GaN MQW microdisk arrays on GaN/Si(111) template. *Phys. stat. sol. (c)* **5**, 2063–2065 (2008).
14. Biswas, K. & Kal, S. Etch characteristics of KOH, TMAH and dual doped TMAH for bulk micromachining of silicon. *Microelectron. J.* **37**, 519–525 (2006).
15. Athanasiou, M. *et al.* Fabrication of two-dimensional InGaN/GaN photonic crystal structure using a modified nanosphere lithography technique. *Appl. Phys. Lett.* **102**, 191108 (2013).
16. Kim, T. *et al.* Coherent nanocavity effect in InGaN/GaN nanodisk arrays. *Appl. Phys. Lett.* **104**, 161108 (2014).
17. Wang, C. F. *et al.* Observation of whispering gallery modes in nanocrystalline diamond Microdisks. *Appl. Phys. Lett.* **90**, 081110 (2007).
18. Liu, X. *et al.* Optically pumped ultraviolet microdisk laser on a silicon substrate. *Appl. Phys. Lett.* 84, 2488 (2004).
19. Reitzenstein, S. *et al.* Lasing in high-Q quantum-dot micropillar cavities. *Appl. Phys. Lett.* **89**, 051107 (2006).
20. Someya, T. *et al.* Room temperature lasing at blue wavelengths in gallium nitride microcavities. *Science* **285**, 1905–1906 (1999).
21. Wang, W. *et al.* Static and dynamic spectroscopy of (Al,Ga)As/GaAs microdisk lasers with interface fluctuation quantum dots. *Phys. Rev. B* **71**, 155306 (2005).
22. Reitzenstein, S. *et al.* Lasing in high-Q quantum dot micropillar cavities. *Appl. Phys. Lett.* **89**, 051107 (2006).
23. Chichibu, S. F. *et al.* Recombination dynamics of localized excitons in cubic phase In$_x$Ga$_{1-x}$N/GaN multiple quantum wells on 3C-SiC/Si (001). *Phys. Stat. Sol. (b)* **234**, 746–749 (2002).
24. Liu, B. *et al.* Great emission enhancement and excitonic recombination dynamics of InGaN/GaN nanorod structures. *App. Phys. Lett.* **103**, 101108 (2013).
25. Smith, R., Liu, B., Bai, J. & Wang, T. Hybrid III-nitride/organic semiconductor nanostructure with high efficiency nonradiative energy transfer for white light emitters. *Nano. Lett.* **13**, 3042–3047 (2013).
26. Christopoulos, S. *et al.* Room-temperature polariton lasing in semiconductor microcavities. *Phys. Rev. Lett.* **98**, 126405(2007).
27. Luo, K. J. *et al.* Dynamics of GaAs/AlGaAs microdisk lasers. *Appl. Phys. Lett.* **77**, 2304 (2000).
28. Zwiller, V. *et al.* Fabrication and time-resolved studies of visible microdisk lasers. *J. Appl. Phys.* **93**, 2307 (2003).
29. Schell, A. W. *et al.* Three-dimensional quantum photonic elements based on single nitrogen vacancy-centres in laser-written microstructures. *Sci. Rep.* **3**, 1577 (2013).
30. Kim, S. S. *et al.* Whispering-gallery-modelike resonance of luminescence from a single hexagonal ZnO microdisk. *J. Appl. Phys.* **106**, 094310 (2009).
31. Imamura, S. *et al.* Optical control of individual carbon nanotube light emitters by spectral double resonance in silicon microdisk resonators. *Appl. Phys. Lett.* **102**, 161102 (2013).
32. Kippenberg, T. J. *et al.* Purcell-factor-enhanced scattering from Si nanocrystals in an optical microcavity. *Phys. Rev. Lett.* **103**, 027406 (2009).
33. Bai, J. *et al.* Mechanisms of dislocation reduction in an Al0.98Ga0.02N layer grown using a porous AlN buffer. *Appl. Phys. Lett.* **93**, 131925 (2006).
34. Wang, T. *et al.* Air-bridged lateral growth of an Al0.98Ga0.02N layer by introduction of porosity in an AlN buffer. *Appl. Phys. Lett.* **87**, 151906 (2005).
35. Bai, J. *et al.* Optical properties of AlGaN/GaN multiple quantum well structure by using a high-temperature AlN buffer on sapphire substrates. *J. of Appl. Phys.* **99**, 023513 (2006).

Acknowledgments

Author contributions

T.W. conceived the idea, organised the project and prepared the manuscript. M.A. fabricated the devices. M.A. performed micro-photoluminescence and time-resolved measurements, confocal PL mapping, and simulations. R.S. and B.L. were involved in time-resolved measurements. M.A. and R.S. contributed to the preparation of the manuscript.

Additional information